

# Mononuclear Fe(II) Complexes Based on the Methylpyrazinyl-Diamine Ligand: Chemical-, Thermo- and Photocontrol of Their Magnetic Switchability

Xue Liu,<sup>†</sup> Jian Zhou,<sup>†</sup> Xin Bao,<sup>\*,†</sup> Zheng Yan,<sup>‡</sup> Guo Peng,<sup>§</sup> Mathieu Rouzières,<sup>||,⊥</sup> Corine Mathonière,<sup>#,¶</sup> Jun-Liang Liu,<sup>||,⊥</sup> and Rodolphe Clérac<sup>\*,||,⊥</sup>

<sup>†</sup>School of Chemical Engineering, Nanjing University of Science and Technology, 210094 Nanjing, P. R. China

<sup>‡</sup>Key Laboratory for Preparation and Application of Ordered Structural Materials of Guangdong Province, Shantou University, Guangdong 515063, P. R. China

<sup>§</sup>Herbert Gleiter Institute of Nanoscience, Nanjing University of Science and Technology, 210094 Nanjing, P. R. China

<sup>||</sup>CNRS, CRPP, UPR 8641, 33600 Pessac, France

<sup>⊥</sup>Univ. Bordeaux, CRPP, UPR 8641, 33600 Pessac, France

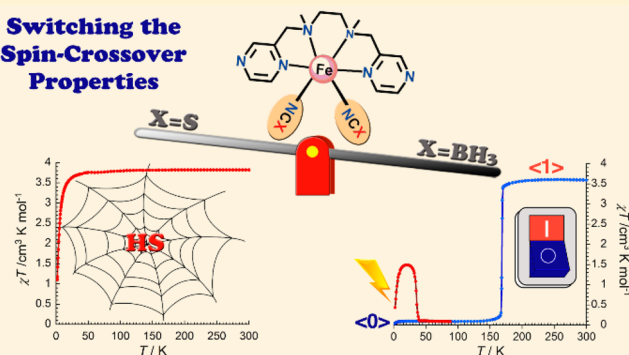
<sup>#</sup>CNRS, ICMCB, UPR 9048, 33600 Pessac, France

<sup>¶</sup>Univ. Bordeaux, ICMCB, UPR 9048, 33600 Pessac, France

## Supporting Information

**ABSTRACT:** Two new mononuclear Fe(II) complexes,  $[\text{Fe}^{(2\text{MeL}_{\text{pz}})}(\text{NCX})_2]$  ( $\text{L} = N,N'$ -dimethyl- $N,N'$ -bis((pyrazin-2-yl)methyl)-1,2-ethanediamine and  $\text{X} = \text{S}$  (1),  $\text{BH}_3$  (2)), have been synthesized and characterized by single-crystal X-ray diffraction, magnetic, optical reflectivity, and photomagnetic measurements. They have similar  $\text{FeN}_6$  coordination environments offered by the tetradentate ligand with a *cis-α* conformation and two  $\text{NCX}^-$  coligands in *cis* positions. However, 1 and 2 have different molecular arrangements and crystal packings, and are isolated in orthorhombic *Pbn* and monoclinic *C2/c* space groups, respectively. 1 remains in a high spin state ( $S = 2$ ) over all temperatures while 2 undergoes a spin transition around 168 K with a small thermal hysteresis of about 0.4 K (at a temperature scan rate of  $1.3 \text{ K min}^{-1}$ ). This phase transition, which can also be optically detected due to the associated marked change of the sample color, occurs between two structurally characterized phases, which exhibit Fe(II) complexes in their high spin and low spin states at high and low temperatures, respectively. The reversible photoswitching between these two states has also been confirmed at low temperatures using well separated wavelength irradiations.

## Switching the Spin-Crossover Properties

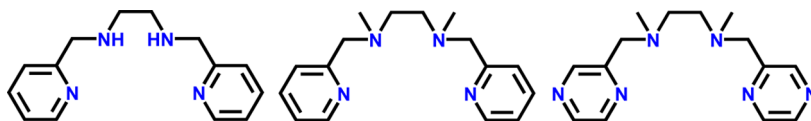


## INTRODUCTION

As one of the most attractive molecule-based switchable materials, spin crossover (SCO) complexes have potential applications as a new generation of advanced materials, such as molecular switches, data storage materials, and data displays.<sup>1</sup> While a spin conversion (SC) relies on a Boltzmann (i.e., thermal) population of the high spin (HS) excited state and thus induces a gradual variation of the physical properties, a first-order spin transition (ST) between a low temperature low spin (LS) phase and a high temperature HS phase is highly desirable to envisage practical applications.<sup>2</sup> Although the electronic configuration (LS versus HS) of the metal center is determined by the magnitude of the energy gap between  $e_g$  and  $t_{2g}$  orbitals and the spin pairing energy at the molecular scale, the elastic interactions, also called cooperativity, between the magnetic centers play a very important role in the bulk magnetic properties. Short- and long-range intermolecular

interactions in the crystal lattice contribute often to high cooperativity and favor the occurrence of an ST, associated with a large thermal hysteresis. However, good control of the cooperativity remains a challenge for synthetic chemists who rely mainly on the tools of crystal engineering, coordination, and supramolecular chemistries. Many efforts have been devoted to the design and synthesis of coordination polymers, inspired by the promising properties of one-dimensional (1D) triazole-based complexes<sup>3</sup> and metallocyanate based coordination polymers.<sup>4</sup> In this approach, the elastic contacts between spin centers are enhanced through bridging ligands. However, spin conversion has been frequently encountered for coordination polymers, indicating the covalent bridge cannot guarantee the occurrence of a spin transition. A discrete

Received: June 7, 2017

Scheme 1. Schematic Structures of the L (left),  $^{2\text{Me}}\text{L}$  (middle), and  $^{2\text{Me}}\text{L}_{\text{pz}}$  (right) Ligands

molecular system can also give rise to first-order spin transition through supramolecular interactions. The mononuclear iron(II) complexes based on Jäger-type ligands are a classic example, as illustrated by  $[\text{FeL}(\text{HIm})_2]$  (L = Butanoic acid, 2,2'-[1,2-phenylenebis(iminomethylidene)]bis[3-oxo-,1,1'-diethyl ester] and HIm = imidazole) which shows a large thermal hysteresis of 70 K owing to a 2D network of hydrogen bonding interactions.<sup>5</sup> Nevertheless, the role of supramolecular interactions toward SC or ST is still ambiguous and extensive studies should be carried out to deepen the overall understanding of the structure–property relationship.

Among various SCO complexes, those based on a neutral tetradentate ligand and  $\text{NCX}^-$  (X = S, Se,  $\text{BH}_3$ ) coligands allow the straightforward formation of neutral mononuclear complexes.<sup>6–9</sup> Pyridine substituted aliphatic amine,<sup>6</sup> Schiff base ligands,<sup>7</sup> and  $\text{N}_4$  embracing ligands with four aromatic donors<sup>8</sup> have all proved their suitability to favor SCO behavior. Many complexes of such type show structural diversity and display polymorphism with different SCO properties, thus allowing a systematic study of the supramolecular interaction role to modulate the SCO behavior. Recently, we have been interested in developing complexes based on a  $N,N'$ -bis(2-pyridylmethyl)-1,2-ethanediamine (L) tetradentate ligand (Scheme 1). The magnetic and photomagnetic behaviors of  $[\text{Fe}(\text{L})(\text{NCS})_2]$  have been studied comprehensively by Létard et al., showing a spin transition between 60 and 70 K.<sup>10</sup> In a more recent work, we substituted the  $\text{NCS}^-$  coligands by  $\text{NCBH}_3^-$ , aiming at chemically tuning the transition temperature. Indeed,  $[\text{Fe}(\text{L})(\text{NCBH}_3)_2]$  exhibits a one-step SC above room temperature and can be in situ converted in air into an LS complex of imine/ $\text{CN}^-$  ligands in solution.<sup>11</sup> We have also studied a structurally related complex  $[\text{Fe}^{(2\text{Me})}\text{L}(\text{NCSe})_2]$  ( $^{2\text{Me}}\text{L} = N,N'$ -dimethyl- $N,N'$ -bis(2-pyridylmethyl)-1,2-ethanediamine) and obtained two polymorphs.<sup>12</sup> One of the these exhibits an unusual hysteretic two-step ST with an ordered  $[\text{HS}–\text{HS}–\text{LS}]$  intermediate phase, while the other polymorph remains HS over all temperatures.

In this work, we are interested to see if using a pyrazine analogue ligand,  $N,N'$ -dimethyl- $N,N'$ -bis(2-pyrazinylmethyl)-1,2-ethanediamine ( $^{2\text{Me}}\text{L}_{\text{pz}}$ , Scheme 1), would lead to a significant modification and thus a chemical tuning of the SCO properties of the resulting iron(II) complexes. It is worth noting that, in some previous reports,<sup>13</sup> the substitution of the pyridine group by pyrazine was found to increase the SCO characteristic temperature (i.e., to favor the low spin state), which was claimed to be induced by a stronger  $\pi$  back-bonding effect of the pyrazine ligand. Herein, we report the syntheses, crystal structures, and magnetic properties of two new mononuclear complexes,  $[\text{Fe}^{(2\text{Me})}\text{L}_{\text{pz}}(\text{NCS})_2]$  (1) and  $[\text{Fe}^{(2\text{Me})}\text{L}_{\text{pz}}(\text{NCBH}_3)_2]$  (2).

## EXPERIMENTAL SECTION

**General.** All reagents obtained from commercial sources were used without further purification. **Safety Note:** Perchlorate salts are potentially explosive, and caution should be taken when dealing with such materials.

**Synthetic Procedures.** *Synthesis of  $N,N'$ -Dimethyl- $N,N'$ -bis(2-pyrazinylmethyl)-1,2-ethanediamine ( $^{2\text{Me}}\text{L}_{\text{pz}}$ ).* To a solution of 4 g

(42.5 mmol) of 2-methyl-pyrazine in 60 mL of tetrachloromethane were added 8.10 g (60.8 mmol) of *N*-chlorosuccinimide and 0.51 g (2.12 mmol) of the catalyst benzoperoxide. The mixture was refluxed for 14 h in the dark. After the reaction was complete (monitored by TLC), the mixture was separated by filtration and the filtrate was concentrated in vacuo giving crude product 2-(chloromethyl)-pyrazine.<sup>14</sup> Then to a solution of 3.24 g (25.6 mmol) of 2-(chloromethyl)-pyrazine in 50 mL of tetrahydrofuran were added 1.1 g (12.2 mmol) of  $N,N'$ -dimethyl-ethylenediamine and 5.1 g (52.0 mmol) of trimethylamine. The mixture was stirred for 24 h at reflux, followed by addition of a 30 mL aqueous solution of 3 M NaOH. After removal of the solvent in vacuum, the dark brown residue was extracted with dichloromethane (30 mL  $\times$  3), then washed with saturated NaCl solution (15 mL), and purified on silica gel. Elution with ethyl acetate/methanol (ratio 10:1) followed by a methanol/ammonia (ratio 10:1) solvent system afforded the  $^{2\text{Me}}\text{L}_{\text{pz}}$  ligand. <sup>1</sup>H NMR (300 MHz,  $\text{CDCl}_3$ )  $\delta$ : 8.69 (s, 2H), 8.52 (m, 2H), 8.47 (m, 2H), 3.75 (s, 4H), 2.68 (s, 4H), 2.31 (s, 6H).

*Synthesis of  $[\text{Fe}^{(2\text{Me})}\text{L}_{\text{pz}}(\text{NCS})_2]$  (1).* To a 20 mL solution of  $^{2\text{Me}}\text{L}_{\text{pz}}$  (0.027 g, 0.1 mmol) in methanol and acetonitrile (ratio 4:1) were added 0.036 g (0.1 mmol) of  $\text{Fe}(\text{ClO}_4)_2 \cdot 6\text{H}_2\text{O}$  and 0.018 g (0.2 mmol) of potassium thiocyanide. The resulting reaction mixture was stirred for 0.5 h, and the yellowish precipitate was filtered. Recrystallization from hot MeCN gave orange flake crystals in 55% yield. IR (KBr,  $\text{cm}^{-1}$ ): 3669 (w), 3083 (w), 3034 (w), 2991 (w), 2965 (w), 2932 (w), 2880 (w), 2809 (w), 2056 (s), 1590 (w), 1524 (w), 1447 (m), 1411 (m), 1366 (m), 1300 (m), 1258 (w), 1193 (w), 1151 (m), 1132 (s), 1019 (m), 966 (m), 929 (w), 859 (m), 838 (m), 808 (m), 778 (m), 753 (m), 680 (w), 639 (w), 593 (w). Elemental analysis, Calcd: C, 43.25; H, 4.54; N, 25.22. Found: C, 43.12; H, 4.38; N, 25.17.

*Synthesis of  $[\text{Fe}^{(2\text{Me})}\text{L}_{\text{pz}}(\text{NCBH}_3)_2]$  (2).* To a 20 mL solution of  $^{2\text{Me}}\text{L}_{\text{pz}}$  (0.027 g, 0.1 mmol) in methanol and dichloromethane (ratio 4:1) were added 0.036 g (0.1 mmol) of  $\text{Fe}(\text{ClO}_4)_2 \cdot 6\text{H}_2\text{O}$  and 0.0124 g (0.2 mmol) of sodium cyanoborohydride. The resulting reaction mixture was stirred for 0.5 h, and the yellowish precipitate was filtered. Recrystallization from hot MeCN gave orange flake crystals in 60% yield. IR (KBr,  $\text{cm}^{-1}$ ): 3675 (w), 3098 (w), 2974 (m), 2893 (m), 2390 (w), 2339 (s), 2314 (m), 2183 (s), 1977 (w), 1719 (w), 1479 (m), 1430 (m), 1412 (s), 1367 (s), 1302 (s), 1227 (w), 1194 (m), 1140 (s), 1119 (s), 1061 (m), 1039 (s), 1021 (m), 970 (m), 943 (w), 855 (s), 841 (s), 809 (m), 668 (w), 636 (w), 595 (m). Elemental analysis, Calcd: C, 47.11; H, 6.42; N, 27.47. Found: C, 47.01; H, 6.31; N, 27.47.

**Physical Characterization.** Magnetic susceptibility measurements of the reported Fe(II) complexes (14.68 mg for 1 and 12.12 mg for 2) were recorded with a Quantum Design MPMS-XL SQUID magnetometer, operating with an applied field of 0.1 and 1.0 T at temperatures from 1.8 to 300 K at rates from 0.01–1.3 K  $\text{min}^{-1}$ . The photomagnetic experiments were performed using a set of photodiodes coupled via an optical fiber to the cavity of a MPMS-7S Quantum Design SQUID magnetometer. Samples of 2 were maintained in a straw between two thin layers of polyethylene films to limit orientation effects. Note that the temperatures have been corrected to take into account the light irradiation heating (an average +2 K has been observed with red light). Experimental susceptibilities were corrected for sample holder and intrinsic diamagnetic contributions. Elemental analyses were performed using an Elementar Vario EL Elemental Analyzer. IR spectra were recorded by the attenuated-total-reflectance (ATR) technique in the range 4000–650  $\text{cm}^{-1}$  using a PerkinElmer Spectrum. DSC measurement was performed on a METTLER TOLEDO DSC1 instrument under a nitrogen atmosphere at a scan rate of 10 K  $\text{min}^{-1}$  in both heating and cooling modes. The surface reflectivity

Table 1. Crystal Data and Refinement Details for 1 and 2

	[Fe( <sup>2Me</sup> L <sub>pzz</sub> )(NCS) <sub>2</sub> ] (1)	[Fe( <sup>2Me</sup> L <sub>pzz</sub> )(NCBH <sub>3</sub> ) <sub>2</sub> ] (2)	
temperature/K	298	123	298
empirical formula	C <sub>16</sub> H <sub>20</sub> FeN <sub>8</sub> S <sub>2</sub>	C <sub>16</sub> H <sub>26</sub> B <sub>2</sub> FeN <sub>8</sub>	C <sub>16</sub> H <sub>26</sub> B <sub>2</sub> FeN <sub>8</sub>
formula weight/g mol <sup>-1</sup>	444.37	407.92	407.92
crystal system	orthorhombic	monoclinic	monoclinic
space group	<i>Pbn</i>	<i>C2/c</i>	<i>C2/c</i>
<i>a</i> /Å	8.1117(13)	19.5442(15)	20.386(2)
<i>b</i> /Å	14.678(2)	7.5846(7)	7.6711(11)
<i>c</i> /Å	17.567(3)	15.6160(12)	15.6307(16)
$\beta$ /deg	90	124.268(2)	123.929(3)
volume/Å <sup>3</sup>	2091.6 (6)	1913.0(3)	2028.2(4)
<i>Z</i>	4	4	4
$\rho_{\text{calc}}$ /mg mm <sup>-3</sup>	1.411	1.416	1.336
$\mu$ /mm <sup>-1</sup>	0.938	0.807	0.761
<i>F</i> (000)	920.0	856.0	856.0
reflections collected	8928	6561	5294
independent reflections	2375	1738	1815
<i>R</i> <sub>int</sub>	0.1068	0.0856	0.0781
goodness-of-fit on <i>F</i> <sup>2</sup>	1.042	1.008	1.026
Final <i>R</i> indexes <sup>a</sup>	<i>R</i> <sub>1</sub> = 0.0673	<i>R</i> <sub>1</sub> = 0.0434	<i>R</i> <sub>1</sub> = 0.0469
[ <i>I</i> ≥ 2σ( <i>I</i> )]	<i>wR</i> <sub>2</sub> = 0.1460	<i>wR</i> <sub>2</sub> = 0.0739	<i>wR</i> <sub>2</sub> = 0.0835
Final <i>R</i> indexes	<i>R</i> <sub>1</sub> = 0.1571	<i>R</i> <sub>1</sub> = 0.0694	<i>R</i> <sub>1</sub> = 0.0844
[all data]	<i>wR</i> <sub>2</sub> = 0.1942	<i>wR</i> <sub>2</sub> = 0.0815	<i>wR</i> <sub>2</sub> = 0.0943

$$^a R_1 = \sum |F_o| - |F_c| / \sum |F_o|. \quad wR_2 = (\sum [w(F_o^2 - F_c^2)^2] / \sum [w(F_o^2)^2])^{1/2}.$$

Table 2. Selected Bond Lengths and Structural Parameters for 1 and 2 (X being S or BH<sub>3</sub>)

	1	2	
<i>T</i> /K	298	123	298
spin state	HS	LS	HS
Fe–N <sub>NCX</sub> /Å	2.092(5)	1.951(3)	2.113(3)
Fe–N <sub>pzz</sub> /Å	2.223(5)	1.975(2)	2.198(2)
Fe–N <sub>amine</sub> /Å	2.272(4)	2.051(2)	2.255(2)
Fe–N <sub>average</sub> /Å	2.19	1.99	2.18
<i>cis</i> N–Fe–N/deg	76.02(16)–103.9(3)	80.69(9)–98.77(9)	75.4(9)–106.3(14)
<i>trans</i> N–Fe–N/deg	163.00(17)–171.4(2)	170.39(9)–178.27 (16)	161.33(9)–173.98(13)
$\Sigma_{\text{Fe}}$ /deg	78.4(8)	60.1(7)	85.7(5)
$\Theta_{\text{Fe}}$ /deg	214.2(16)	180.4(11)	254.8(10)
N–C–X/deg	179.0(6)	175.0(3)	177.3(4)
Fe–N–C <sub>NCX</sub> /deg	166.2(5)	167.3(2)	162.8(3)

measurements have been performed with a home-built system, operating between 10 and 300 K and in the spectrometric range 400–1000 nm. A halogen-tungsten light source (Leica CLS 150 XD tungsten halogen source adjustable from 0.05 mW cm<sup>-2</sup> to 1 W cm<sup>-2</sup>) was used as the spectroscopic light. The measurements were calibrated by a NIST traceable standard for reflectance (sphereOptics, ref SG3054). As the samples are potentially very photosensitive, the light exposure time was minimized during the experiments keeping the samples in the dark except during the spectra measurements when white light is shined on the sample surface (*P* = 1 mW cm<sup>-2</sup>). For all the excitation/de-excitation experiments performed at 10 K, the sample was initially placed at this temperature keeping the sample in the dark to avoid any excitation. Heating and cooling measurements were carried out at 4 K min<sup>-1</sup>. For white light irradiation, the source described above was used, but in a continuous manner with a power of 1 mW/cm<sup>2</sup>. Light Emitting Diodes (LEDs) operating between 365 and 1050 nm (from Thorlabs) were used for excitation experiments.

**Single Crystal X-ray Diffraction.** Single-crystal X-ray data were collected on a Bruker D8 Quest diffractometer or a Rigaku R-Axis SPIDER IP diffractometer using graphite monochromated Mo *K* $\alpha$  radiation ( $\lambda$  = 0.71073 Å). A multiscan absorption correction was

performed. The structures were solved using direct methods and refined by full-matrix least-squares on *F*<sup>2</sup> using SHELXS and SHELXL<sup>15</sup> and the graphical user interface Olex2.<sup>16</sup> Non-hydrogen atoms were refined anisotropically, and hydrogen atoms were placed in calculated positions refined using idealized geometries (riding model) and assigned fixed isotropic displacement parameters. CCDC 1553897–1553899 contain the supplementary crystallographic data for this paper. These data can be obtained free of charge from The Cambridge Crystallographic Data Centre via [www.ccdc.cam.ac.uk/data\\_request/cif](http://www.ccdc.cam.ac.uk/data_request/cif).

## RESULTS AND DISCUSSION

**Synthesis and Characterization.** Reaction of <sup>2Me</sup>L<sub>pzz</sub>, Fe(CIO<sub>4</sub>)<sub>2</sub>·6H<sub>2</sub>O and KNCS or NaNCBH<sub>3</sub> in a mixture solvent of MeOH and CH<sub>2</sub>Cl<sub>2</sub>/MeCN results in fast precipitation of **1** and **2**, respectively. Similar to our previously reported analogues,<sup>11,12</sup> **1** and **2** have low solubility at room temperature in MeOH and EtOH. Therefore, single crystals were obtained by recrystallization of those precipitates from hot MeCN.

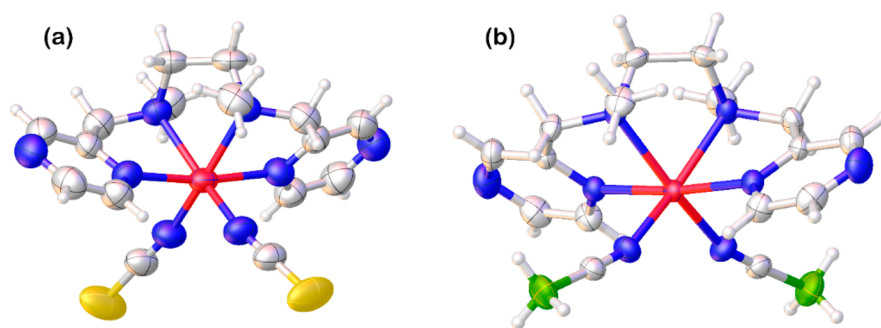


**Figure 1.** View of the molecular structures of the Fe(II) complex in **1** (a) and **2** (b) at 298 K. Thermal ellipsoids are presented at 50% probability. Color code: Fe, red; C, gray; H, white; S, yellow; B, green; N, blue.

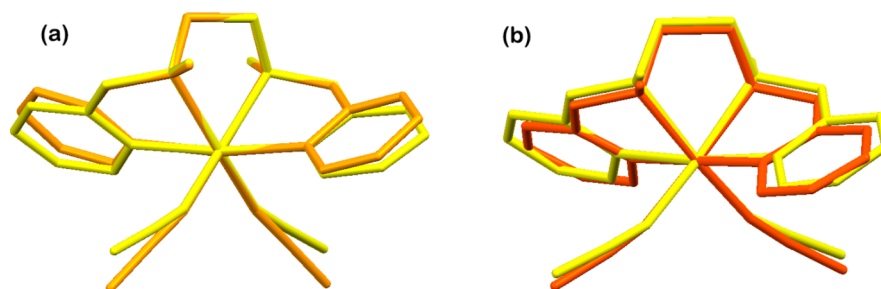


**Figure 2.** Overlay of the molecular structures of the Fe(II) complex in (a) **1** (orange) and **2** (yellow) at 298 K; (b) **2** at 123 K (red) and 298 K (yellow), showing different arrangements of both  $2\text{MeL}_{\text{pz}}$  and  $\text{NCX}^-$  ligands (X being S or  $\text{BH}_3$ ).

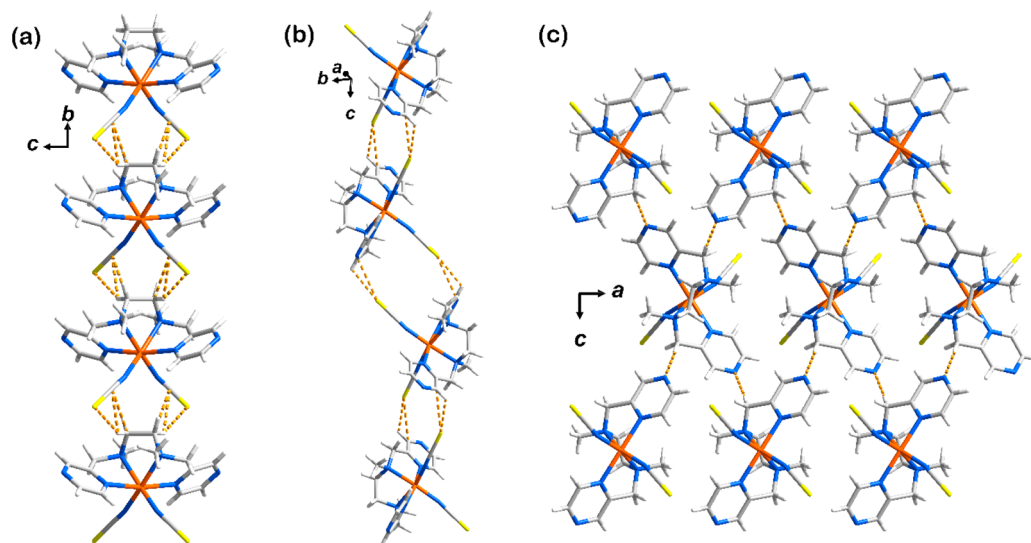


**Figure 3.** Packing diagrams of **1** showing the 1D supramolecular arrangement (a and b) and the 2D corrugated layer packed in the  $ac$  plane (c). Color code: C, light gray; H, gray; Fe, orange; N, blue; S, yellow. Short interactions are indicated by dotted lines.

Solid-state infrared (IR) spectra were recorded for **1** and **2** at room temperature (Figure S1). For complexes which contain  $\text{NCS}^-$  anions, the region of the  $\text{C}\equiv\text{N}$  stretch frequency is particularly useful in characterizing the spin state of the iron(II) center. It has been demonstrated that the N-bound HS complex normally shows absorption between 2020 and 2080  $\text{cm}^{-1}$ , whereas a band at  $\sim 2100$   $\text{cm}^{-1}$  denotes an LS ground state.<sup>17</sup> For **1**, the stretching mode at 2056  $\text{cm}^{-1}$  falls within the range for HS species. Fe(II) complexes containing  $\text{NCBH}_3^-$  are relatively rare, and most of them are HS at room temperature, showing  $\text{C}\equiv\text{N}$  stretch around 2180–2190  $\text{cm}^{-1}$ .<sup>17b,18</sup> One example in an HS/LS mixed state shows a stretch at 2192  $\text{cm}^{-1}$ .<sup>19</sup> In our previous report, we showed that  $[\text{Fe}(\text{L}-$

$\text{NCBH}_3)_2]$  is an LS complex at room temperature and shows a band at 2203  $\text{cm}^{-1}$ .<sup>11</sup> In complex **2**, the corresponding band observed at 2183  $\text{cm}^{-1}$  is in good agreement with HS complexes. The multibands around 2310  $\text{cm}^{-1}$  are ascribed to B–H stretches.

**Crystal Structures.** The crystal structures were determined at 298 K (**1** and **2**) and 123 K (**1**). The crystallographic data and refinement parameters are listed in Tables 1 and 2. Complex **1** crystallizes in the orthorhombic  $Pbnm$  space group while the monoclinic  $C2/c$  space group is observed for **2**. The asymmetric unit contains half of an Fe(II) complex centered on a 2-fold axis. As shown in Figures 1, S2, and S3, the tetradentate ligand wraps an iron(II) metal ion in a  $\text{cis-}\alpha$  conformation,

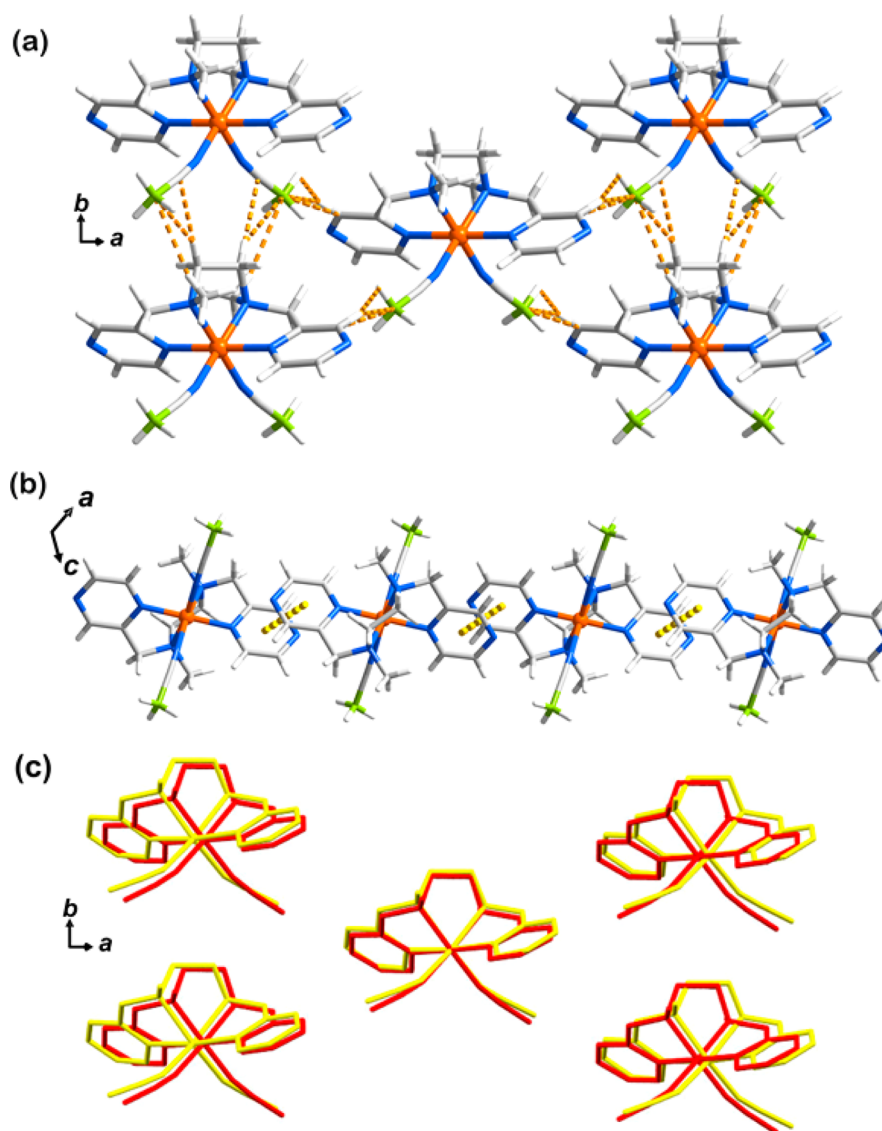


**Figure 4.** Packing diagrams of **2** showing (a) the flat layer packed in the *ab* plane and (b) the 1D supramolecular arrangement connected by pyrazine  $\pi\cdots\pi$  interactions. Color code: C, light gray; H, gray; Fe, orange; N, blue; B, green. Short interactions are indicated by dotted lines. (c) Overlay of crystal packing in the *ab* plane at 123 K (red) and 298 K (yellow).

leaving two *cis* positions for  $\text{NCX}^-$  coligands. As imposed by the tetradentate ligand, the Fe(II) center can adopt either  $\Delta$  or  $\Lambda$  chirality leading to racemic compounds.

The average value of the six Fe–N bond lengths determined at 298 K (2.19 Å for **1** and 2.18 Å for **2**) falls within the range expected for HS Fe(II) complexes with octahedral geometry, in agreement with IR spectroscopy data. Upon cooling to 123 K, the average Fe–N bond length of **2** decreases dramatically to 1.99 Å due to the spin state change from HS to LS state. The octahedral distortion parameters  $\Sigma$  and  $\Theta$  ( $\Sigma$  is the sum of deviations from  $90^\circ$  of the 12 *cis* N–Fe–N angles;  $\Theta$  is the sum of the deviations from  $60^\circ$  of the 24 possible octahedron twist angles; i.e.,  $\Sigma = 0$  and  $\Theta = 0$  are corresponding to a perfect octahedral site)<sup>20</sup> at 298 K indicate that the Fe(II) site in **2** ( $\Sigma = 85.7(5)^\circ$  and  $\Theta = 254.8(10)^\circ$ ) has a more distorted  $\text{N}_6$  coordination sphere than in **1** ( $\Sigma = 78.4(8)^\circ$  and  $\Theta = 214.2(16)^\circ$ ). At 123 K, the  $\Sigma$  and  $\Theta$  values for **2** decrease significantly to  $60.1(7)^\circ$  and  $180.4(11)^\circ$ , respectively, corresponding to a more regular octahedral geometry in the LS state. Overlay of the molecular structures of the Fe(II) complex in **2**

at 298 and 123 K (Figure 2b) shows not only the shrinkage of Fe–N bond lengths but also rearrangement of the tetradentate and  $\text{NCX}^-$  ligands. Compared with aliphatic amine, the pyrazine ring moves closer to the metal ion center, as reflected by a larger variation in Fe–N<sub>pyrazine</sub> (0.22 Å) bond length than Fe–N<sub>amine</sub> (0.20 Å). The two  $\text{NCX}^-$  groups also move closer upon thermal spin crossover from HS to LS, with the angle defined by the two linear  $\text{NCX}^-$  ligands of  $138.2^\circ$  at 298 K to  $128.2^\circ$  at 123 K, respectively. Accordingly, the Fe–N≡C angle at 123 K deviates from the ideal  $180^\circ$  to a smaller extent ( $162.8(3)^\circ$  versus  $167.3(2)^\circ$  at 298 and 123 K respectively). The superposition of the Fe(II) complex in **1** and **2** (Figure 2a) at 298 K shows main differences arising from different coordination orientations of the  $\text{NCX}^-$  ligand and pyrazine ring. The angle between the two  $\text{NCX}^-$  groups in **1** ( $106.5^\circ$ ) is much smaller than that in **2** ( $138.2^\circ$ ).

As shown in Figure 3a and 3b, each  $[\text{Fe}^{2\text{Me}}\text{L}_{\text{pz}}(\text{NCS})_2]$  unit embraces a second molecule by its two  $\text{NCS}^-$  arms in **1**, forming a 1D supramolecular organization along the *b* axis with short van der Waals interactions,  $\text{S1}\cdots\text{H6A}$  (2.9178(23) Å),

C8⋯H6A (2.7684(59) Å), and C6⋯C8 (3.3498(77) Å), which were found between adjacent molecules. Besides, S1⋯H3 (2.9368(24) Å) and S1⋯C3 (3.4545(72) Å) interactions between lateral molecules also link them into a supramolecular chain. The Fe(II) complexes with  $\Delta$  and  $\Lambda$  chirality propagate alternatively along the above two supramolecular chains. A homochiral layer parallel to the *ac* plane is formed by N2⋯H5B (2.5941(57) Å) intermolecular interactions emphasizing the key role of the pyrazine group in the establishment of a dense supramolecular network in **1** (Figure 3c).

As shown in Figure 4, the crystal packing of **2** is quite different. Homochiral Fe(II) complexes pack in the *ab* plane via multiple intermolecular interactions involving pyrazine rings, ethyl groups, and NCBH<sub>3</sub><sup>−</sup> coligands. The overlay of crystal packings at 298 and 123 K in this crystallographic plane shows clearly a large rearrangement of the lattice associated with the spin transition, which has not been observed in our previously reported [Fe<sup>2Me</sup>L(NCSe)<sub>2</sub>] and [FeL(NCBH<sub>3</sub>)<sub>2</sub>] analogues.<sup>11,12</sup> The reduction of the Fe(II) coordination sphere volume at the transition induces a significant modification of intermolecular interactions. Upon cooling from 298 to 123 K, the intermolecular C8⋯H6B, B1⋯H6B, B1⋯H7B, B1⋯H3, and H1C⋯H3 short interactions decrease notably, with corresponding values of 2.875(35)/2.5912(33), 3.6607(71)/3.1975(51), 3.1388(52)/2.9638(39), 2.8885(77)/2.8405(54), and 2.5220(2)/2.3946(1) Å at 298/123 K, respectively. Additionally, the pyrazine groups form strong  $\pi\cdots\pi$  interactions between adjacent complexes leading to a 1D supramolecular organization with alternating chirality (Figure 4b). The centroid distance between the two pyrazine rings does not change significantly upon spin state change with values of 3.6140(4)/3.6681(2) Å at 298/123 K, respectively. The dense crystal structure in **2** involving numerous supramolecular interactions, favored in part by the presence of the pyrazine groups, plays an important role in enhancing the elastic interactions (i.e., cooperativity) between the switchable Fe(II) sites and thus naturally favor the occurrence of a first-order phase transition in agreement with the structural data and the absence of symmetry breaking (see Table 1).

The thermal stability of the two complexes were analyzed on crystalline samples by thermogravimetric analyses (TGA) from 30 to 800 °C at a rate of 10 K min<sup>−1</sup> under a N<sub>2</sub> atmosphere (Figure S4). The curves show that they are stable up to 250 and 300 °C, respectively. No weight loss was observed before decomposition, confirming the absence of interstitial solvent molecules in both compounds. The impressive thermal stability of this family of mononuclear complexes is likely the result of the strong chelating effect of the tetradentate <sup>2Me</sup>L<sub>pz</sub> ligand and the dense supramolecular network.

**Magnetic Susceptibility Studies.** Magnetic susceptibility data were recorded on polycrystalline samples between 1.8 and 300 K in both cooling and heating modes. The results are shown in Figure 5 in the form of  $\chi T$  versus *T* plots (where  $\chi$  is molar magnetic susceptibility and *T* is temperature). The  $\chi T$  value of **1** at 300 K is 3.8 cm<sup>3</sup> K mol<sup>−1</sup>, lying in the range typically observed for Fe(II) ion in the HS state. This value remains relatively constant until 50 K. Below this temperature, the  $\chi T$  value decreases rapidly to 1.1 cm<sup>3</sup> K mol<sup>−1</sup> at 1.85 K, probably due to the magnetic anisotropy of the Fe(II) ion and/or intermolecular antiferromagnetic interactions.

The  $\chi T$  product of **2** is 3.6 cm<sup>3</sup> K mol<sup>−1</sup> at 300 K and decreases slightly to 3.4 cm<sup>3</sup> K mol<sup>−1</sup> at 171 K, indicating the presence of HS Fe(II) ion sites. Upon further cooling, the  $\chi T$

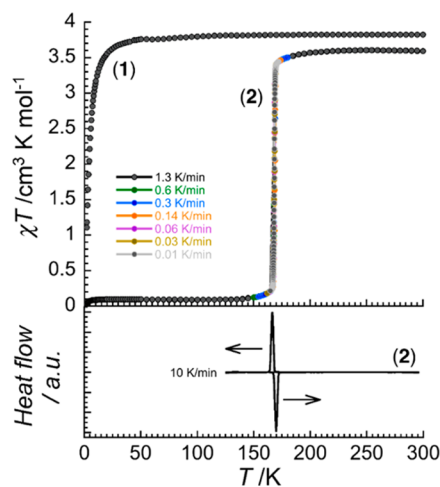


**Figure 5.** Top: Temperature dependence of the  $\chi T$  product ( $\chi$  being the magnetic susceptibility defined as  $M/H$  per mole of complex) at 0.1 T for **1** and 1 T for **2**; the temperature scan rate is indicated in the figure. Bottom: differential scanning calorimetry (DSC) thermograms for **2** at 10 K min<sup>−1</sup>.

value drops sharply to 0.2 cm<sup>3</sup> K mol<sup>−1</sup> at 166 K, and slightly further to 0.1 cm<sup>3</sup> K mol<sup>−1</sup> in the 145–10 K range. This behavior is associated with an almost complete one-step spin transition from an HS ( $S = 2$ ) to an LS ( $S = 0$ ) phase as the low temperature  $\chi T$  value corresponds to less than 3% of residual HS Fe(II) centers. Below 10 K, the small decrease of the  $\chi T$  product is probably due to the zero-field-splitting of residual HS Fe(II). The magnetic measurements performed in the subsequent heating mode revealed a narrow thermal hysteresis of 0.4 K at a scan rate of 1.3 K min<sup>−1</sup>, associated with the observed first-order transition. The experimental  $\chi T$  versus *T* curve can be fitted to the domain model (see Figure S12 for details)<sup>22</sup> with a number of interacting Fe(II) complex per domain of 51.0, underlying the strong cooperativity present in this system. The limit temperatures of this hysteresis (determined as the temperatures for which 50% of the spins are converted) are  $T_{1/2 \downarrow} = 168.2$  K,  $T_{1/2 \uparrow} = 168.6$  K in the cooling and warming modes, respectively. More over, it is worth noting that the width of thermal hysteresis is small and thus not very sensitive to the scan rate between 1.3 K min<sup>−1</sup> (0.4 K) and 0.01 K min<sup>−1</sup> (0.2 K) (Figure S5).

The study of complex **2** by differential scanning calorimetry (DSC; bottom part of Figure 5) confirms the presence of a first-order phase transition associated with the SCO process, in good agreement with the magnetic measurements and the numerous supramolecular interactions (vide supra). Upon cooling/heating at 10 K min<sup>−1</sup>, exothermic/endothermic peaks were observed at 166.5/169.8 K. The thermal hysteresis observed by DSC (3.3 K) is wider than by magnetic measurement as a result of the faster temperature scan rate. The corresponding  $\Delta H$  and  $\Delta S$  values were estimated to be 6.85/6.85 kJ mol<sup>−1</sup> and 41.11/40.34 J K<sup>−1</sup> mol<sup>−1</sup> respectively. These values are within the experimental range generally observed for analogue Fe(II) SCO complexes.<sup>23</sup>

**Optical Reflectivity and Photomagnetic Studies.** Optical reflectivity and photomagnetic studies were carried out on complex **2**. Changes in the reflectivity spectra measured as a function of temperature were used to monitor the relative amounts of HS and LS iron(II) species. As shown in Figure 6, the absorption band intensity with a maximum around 850 nm

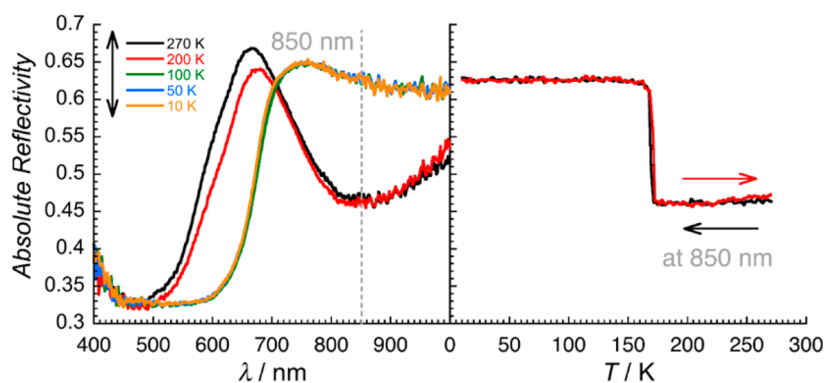


**Figure 6.** Left: Selected reflectivity spectra emphasizing the reversible temperature dependence of the optical properties of **2**. Right: Thermal evolution of reflectivity signal at 850 nm between 10 and 270 K. A white halogen light was used as a spectroscopic source with a power of  $0.8 \text{ mW cm}^{-2}$ , and the temperature scan rate was  $4 \text{ K min}^{-1}$ .

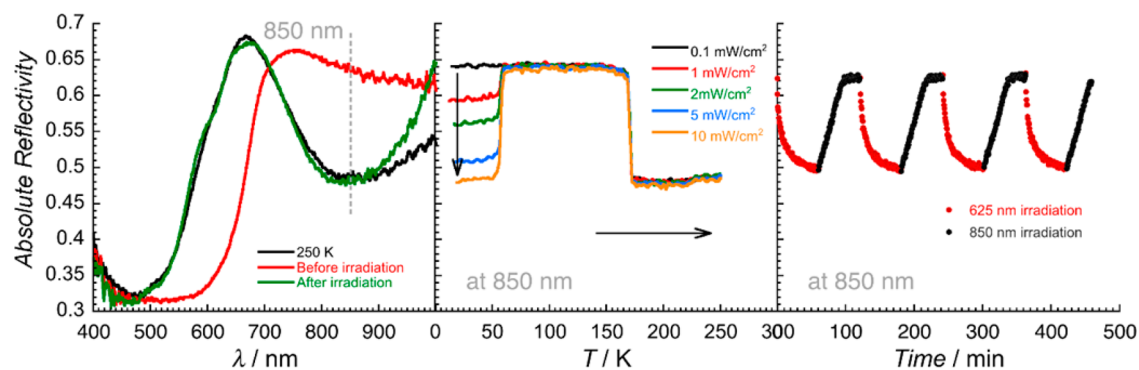


**Figure 7.** Left: Comparison of the reflectivity spectra at 250 K (black), at 10 K before irradiation (red) and after 30 min of excitation with a 625-nm LED ( $10 \text{ mW cm}^{-2}$ , green). Middle: Thermal variation of the reflectivity signal recorded at 850 nm increasing the temperature in dark at  $4 \text{ K min}^{-1}$  after irradiation by a 625-nm LED at 10 K for 30 min (with different light power from 0.1 to  $10 \text{ mW cm}^{-2}$ ). Right: Time evolution of the absolute reflectivity recorded at 850 nm under successive irradiations at 10 K (at  $4 \text{ mW cm}^{-2}$ ) by 625-nm (red ●) and 850-nm (black ●) LEDs showing the good reversibility of the photo induced spin state switching.

(attributed to  ${}^5T_2 \rightarrow {}^5E$  d–d transition of the HS Fe(II)) decreases markedly upon cooling and, concomitantly, the absorption band near 650 nm (tentatively assigned to both  ${}^1A_1 \rightarrow {}^1T_1$  d–d and MLCT transitions of the Fe(II) complex in its LS state) increases. These spectral changes are reversible in the subsequent warming/cooling cycles. Thermal variation of the absolute reflectivity recorded at 850 nm clearly confirms a spin transition with  $T_{1/2 \downarrow} = 168 \text{ K}$ ,  $T_{1/2 \uparrow} = 171 \text{ K}$ , in good agreement with magnetic studies (Figures 6 and S6).

Irradiation with white light ( $0.8 \text{ mW cm}^{-2}$ ) at 10 K did not change the spectrum significantly, indicating that the complex is not very photosensitive to broad white light exposure (Figure S7).<sup>24</sup> Hence different wavelengths from 365 to 1050 nm were tested as excitation light and those between 505 and 660 nm were found to be very efficient to undergo LS to HS photoconversion (Figure S8). A 625-nm LED was used in the following measurements, as it possesses the highest irradiation power in our setup. As seen in Figure 7, after 30 min of irradiation at 10 K with a power of  $10 \text{ mW cm}^{-2}$  (the highest available power that is also the most efficient one), the spectrum of the HS phase is completely recovered. In the subsequent warming of the sample at  $4 \text{ K min}^{-1}$ , the photoinduced excited HS phase relaxes fully at 60 K. Interestingly, this complex also presents reverse photoswitchability. In the 365–1050 nm range, the 850-nm LED is the most efficient source to de-excite the photoinduced state (Figure S9). Remarkably, the photoexcited HS state can be

reversibly switched on and off by 625- and 850-nm irradiations over many cycles (right part of Figure 7).

The photoswitching between the LS and HS phases for **2** was also monitored by photomagnetic measurements (Figure 8). First, the sample was cooled in the dark down to 10 at  $0.3 \text{ K min}^{-1}$

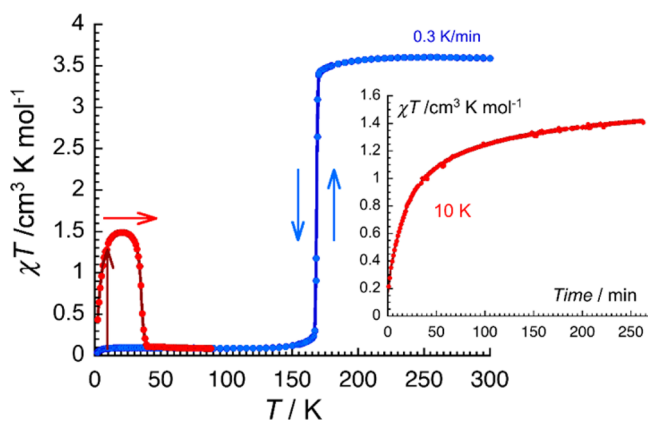


**Figure 8.** Temperature dependence of the  $\chi T$  product ( $\chi$  being the magnetic susceptibility defined as  $M/H$  per mole of complex) at 1 T for **2** in the dark (blue dotted line) and after photoexcitation of a 650 nm LED (at  $1.5 \text{ mW cm}^{-2}$ ) with a temperature scan rate of  $0.3 \text{ K min}^{-1}$  (red dotted line). Inset: Time evolution of the  $\chi T$  product at 10 K during the photoexcitation with a 650 nm LED (at  $1.5 \text{ mW cm}^{-2}$ ).

$\text{min}^{-1}$ . Upon red light irradiation ( $650 \text{ nm}$ ,  $1.5 \text{ mW cm}^{-2}$ ), the  $\chi T$  product increases with time and reaches, after 260 min,  $1.42 \text{ cm}^3 \text{ K mol}^{-1}$ , a value that is still far from the expected saturation for the HS phase. So the photoconversion that is quantitatively seen by optical reflectivity is efficiently occurring at the surface and is rather much less efficient at the bulk level. After the irradiation was turned off, the sample was warmed up at  $0.3 \text{ K min}^{-1}$ . The initial increase of the  $\chi T$  product is associated with the zero-field splitting effect of the photo-induced HS Fe(II) centers which fully relax around 40 K.

**Discussion of the Magnetic Property in Relation with the Molecular and Crystal Structures.** Including the two new complexes discussed here, the crystal structure of six Fe(II) complexes of this family with a related tetradentate ligand (see Scheme 1) and  $\text{NCX}^-$  coligands have been reported: (i)  $[\text{FeL}(\text{NCS})_2]$  that crystallizes in the  $P2_1/n$  space group and shows a spin transition between 60 and 70 K;<sup>10</sup> (ii)  $[\text{FeL}(\text{NCBH}_3)_2]$ <sup>11</sup> and (iii)  $[\text{Fe}^{2\text{Me}}\text{L}(\text{NCSe})_2]$ <sup>12</sup> (polymorph a), which are isostructural and crystallize in the  $Aba2$  space group, with the former complex showing a spin conversion above room temperature, while the latter exhibits a thermal hysteresis with a two-step spin transition below 130 K; and finally (iv)  $[\text{Fe}^{2\text{Me}}\text{L}(\text{NCSe})_2]$  (polymorph b) that is isostructural to 2 but stays in its HS state above 1.8 K.<sup>12</sup> A careful comparison of those structures shows that the monodentate  $\text{NCX}^-$  coligands are flexible and can adopt different coordination orientations, while the observed geometry of tetradentate ligands around the Fe(II) site is really consistent along this family of complexes as expected due to the geometrical restriction imposed in the chelating mode. Clarifying the electronic effect of the tetradentate ligand modifications (pyrazine versus pyridine, bis-methylated or not) by comparison of these complexes is not an easy task as other variations in coligand, molecular arrangement, and crystal packing (vide infra) have also an impact on the overall magnetic properties of the materials. Nevertheless, in order to probe the local influence of the ligand modifications (i.e., pyrazine versus pyridine and  $\text{NCS}^-$  versus  $\text{NCBH}_3^-$ ) on the ligand field strength, the optical spectra for the  $[\text{NiL}(\text{NCX})_2]$  analogous complexes ( $\text{L} = {}^{2\text{Me}}\text{L}$  or  ${}^{2\text{Me}}\text{L}_{\text{pz}}$  and  $\text{X} = \text{S}$  or  $\text{BH}_3$ ; in  $\text{CH}_3\text{CN}$ ) have been compared in the range of the  ${}^3\text{A}_{2\text{g}} \rightarrow {}^3\text{T}_{2\text{g}}$  transition allowing direct access to the ligand field splitting ( $10\text{Dq}$ ).<sup>21</sup> From these spectra (Figure S11), the  $10\text{Dq}$  values for  $[\text{Ni}({}^{2\text{Me}}\text{L})(\text{NCS})_2]$ ,  $[\text{Ni}({}^{2\text{Me}}\text{L}_{\text{pz}})(\text{NCS})_2]$ ,  $[\text{Ni}({}^{2\text{Me}}\text{L})(\text{NCBH}_3)_2]$ , and  $[\text{Ni}({}^{2\text{Me}}\text{L}_{\text{pz}})(\text{NCBH}_3)_2]$  complexes are found to be  $10735(70)$ ,  $10760(120)$ ,  $11182(140)$ , and  $11187(60) \text{ cm}^{-1}$ , respectively, suggesting that the substitution of the pyridine group in  ${}^{2\text{Me}}\text{L}$  by a pyrazine one in  ${}^{2\text{Me}}\text{L}_{\text{pz}}$  does not significantly modify the ligand field strength. In contrast, the replacement of  $\text{NCS}^-$  by  $\text{NCBH}_3^-$  results in a blue shift of about  $430 \text{ cm}^{-1}$ , confirming that  $\text{NCS}^-$  coligands impose a weaker ligand field to the metal ion and thus favor the stabilization of the high spin state in 1. Again it must be emphasized that the conclusions from these solution measurements on analogous complexes might not be conserved in the solid state, as the crystal packing and intermolecular interactions are well-known to significantly alter the metal ion coordination sphere and consequently the magnetic properties. By extending the discussion to the crystal packing, it is very clear that these complexes are involved in different sets of supramolecular interactions and organizations. Nevertheless, in all cases, a very dense crystal packing without interstitial solvent molecules and with multiple intermolecular interactions

between  $\text{NCX}^-$  and tetradentate ligands are recurrent characteristics of these SCO systems. It is also worth noting that  $\pi \cdots \pi$  interactions are observed in three of the four highly cooperative SCO complexes (which display a spin transition), emphasizing their key role in increasing elastic interactions between Fe(II) molecules and thus the cooperativity.

## CONCLUSIONS

In the present report, two mononuclear Fe(II) complexes based on the methylpyrazinyl-diamine tetradentate ligand have been synthesized and characterized.  $\text{NCS}^-$  and  $\text{NCBH}_3^-$  coligands were used to adjust the ligand field strength around the Fe(II) center. Although 1 and 2 have quite similar compositions, they crystallize in different space groups and have different molecular arrangements and crystal packings. Complex 1 is stabilized in its HS state over the entire temperature range in agreement with the presence of  $\text{NCS}^-$  coligands, which impose a weaker ligand field strength to the metal ion than  $\text{NCBH}_3^-$  (see Figure S11). In contrast, complex 2 undergoes a one-step spin transition around 168 K with an extremely small thermal hysteresis. As shown by the structural analysis of 2, the dense network of supramolecular contacts, favored by the presence of pyrazine groups, is creating strong elastic interactions (i.e., cooperativity) between the switchable Fe(II) complexes in the solid. As a consequence, the resulting phase transition is strongly of first-order nature as illustrated by the large rearrangements of the molecular structure and the crystal packing, and the remarkably abrupt and one-step switching of the magnetic and optical properties, which is unprecedented in this family of SCO complexes. The spin state switching of the complex 2 can also be photocontrolled and cycled back and forth by using selected and well separated wavelength irradiation in the red ( $625\text{--}650 \text{ nm}$ ) and near-infrared ( $850 \text{ nm}$ ) regions. The present work together with our previous reports<sup>9,12</sup> confirms that this pyrazine-based tetradentate  $\text{N}_4$  ligand (Scheme 1) is a good candidate to design new thermally and photoswitchable SCO complexes but that the choice of the  $\text{NCX}^-$  coligand to adjust the ligand field strength is also critical. In addition, it should be emphasized that the pyrazine group of the  ${}^{2\text{Me}}\text{L}_{\text{pz}}$  ligand favors remarkably dense supramolecular interactions and thus first-order spin transition allowing a “sharp” switching of the magnetic and optical properties.

## ASSOCIATED CONTENT

### Supporting Information

The Supporting Information is available free of charge on the ACS Publications website at DOI: 10.1021/acs.inorgchem.7b01430.

IR spectra, view of molecular structures, TG curves, additional magnetic and reflectivity spectra of 2 (PDF)

### Accession Codes

CCDC 1553897–1553899 contain the supplementary crystallographic data for this paper. These data can be obtained free of charge via [www.ccdc.cam.ac.uk/data\\_request/cif](http://www.ccdc.cam.ac.uk/data_request/cif), or by emailing [data\\_request@ccdc.cam.ac.uk](mailto:data_request@ccdc.cam.ac.uk), or by contacting The Cambridge Crystallographic Data Centre, 12 Union Road, Cambridge CB2 1EZ, UK; fax: +44 1223 336033.

## AUTHOR INFORMATION

### Corresponding Authors

\*E-mail: [baox199@126.com](mailto:baox199@126.com) (X.B.).

\*E-mail: [clerac@crpp-bordeaux.cnrs.fr](mailto:clerac@crpp-bordeaux.cnrs.fr) (R.C.).

ORCID 

Xin Bao: 0000-0002-2725-0195

Jun-Liang Liu: 0000-0002-5811-6300

## Notes

The authors declare no competing financial interest.

## ACKNOWLEDGMENTS

This work was supported by the National Natural Science Foundation of China (21401104), the Natural Science Foundation of Jiangsu Province (BK20140774), the Fundamental Research Funds for the Central Universities (30920140111002), and financial support from State Key Laboratory of Coordination Chemistry of Nanjing University. Z.Y. is thankful for the financial support from the NSFC (21501067) and the Zhejiang Provincial Natural Science Foundation of China (Grant LQ15B010002). R.C., C.M., and M.R. thank the University of Bordeaux, the CNRS, the Nouvelle Aquitaine Région, the MOLSPIN COST action CA15128, and the GdR MCM-2: Magnétisme et Commutation Moléculaires.

## REFERENCES

- (1) Kahn, O.; Martinez, C. J. Spin-Transition Polymers: From Molecular Materials Toward Memory Devices. *Science* **1998**, *279*, 44–48.
- (2) (a) Gütllich, P.; Garcia, Y.; Woike, T. Photoswitchable Coordination Compounds. *Coord. Chem. Rev.* **2001**, *219*, 839–879. (b) Bousseksou, A.; Molnár, G.; Matouzenko, G. Switching of Molecular Spin States in Inorganic Complexes by Temperature, Pressure, Magnetic Field and Light: Towards Molecular Devices. *Eur. J. Inorg. Chem.* **2004**, 4353–4369. (c) Gütllich, P.; Ksenofontov, V.; Gaspar, A. B. Pressure effect studies on spin crossover systems. *Coord. Chem. Rev.* **2005**, *249*, 1811–1829. (d) Real, J. A.; Gaspar, A. B.; Muñoz, M. C. Thermal, Pressure and Light Switchable Spin-Crossover Materials. *Dalton Trans.* **2005**, 2062–2079. (e) Sato, O.; Tao, J.; Zhang, Y. Z. Control of Magnetic Properties through External Stimuli. *Angew. Chem., Int. Ed.* **2007**, *46*, 2152–2187.
- (3) (a) Kitchen, J. A.; Brooker, S. Spin Crossover in Iron(II) Complexes of 3,5-di(2-pyridyl)-1,2,4-triazoles and 3,5-di(2-pyridyl)-1,2,4-triazolates. *Coord. Chem. Rev.* **2008**, *252*, 2072–2092. (b) Aromí, G.; Barrios, L. A.; Roubeau, O.; Gamez, P. Triazoles and Tetrazoles: Prime Ligands to Generate Remarkable Coordination Materials. *Coord. Chem. Rev.* **2011**, *255*, 485–546.
- (4) Muñoz, M. C.; Real, J. A. Thermo-, Piezo-, Photo- and Chemo-switchable Spin Crossover Iron(II)-Metalloacyanate Based Coordination Polymers. *Coord. Chem. Rev.* **2011**, *255*, 2068–2093.
- (5) Weber, B.; Bauer, W.; Obel, J. An Iron(II) Spin-Crossover Complex with a 70 K Wide Thermal Hysteresis Loop. *Angew. Chem., Int. Ed.* **2008**, *47*, 10098–10101.
- (6) (a) Matouzenko, G. S.; Bousseksou, A.; Lecocq, S.; van Koningsbruggen, P. J.; Perrin, M.; Kahn, O.; Collet, A. Spin Transition in [Fe(DPEA)(NCS)<sub>2</sub>], a Compound with the New Tetradentate Ligand (2-Aminoethyl)bis(2-pyridylmethyl)amine (DPEA): Crystal Structure, Magnetic Properties, and Mössbauer Spectroscopy. *Inorg. Chem.* **1997**, *36*, 2975–2981. (b) Matouzenko, G. S.; Bousseksou, A.; Lecocq, S.; van Koningsbruggen, P. J.; Perrin, M.; Kahn, O.; Collet, A. Polymorphism in Spin Transition Systems. Crystal Structure, Magnetic Properties, and Mössbauer Spectroscopy of Three Polymorphic Modifications of [Fe(DPPA)(NCS)<sub>2</sub>] [DPPA = (3-Aminopropyl)bis(2-pyridylmethyl)amine]. *Inorg. Chem.* **1997**, *36*, 5869–5879. (c) Li, B.; Wei, R. J.; Tao, J.; Huang, R. B.; Zheng, L. S.; Zheng, Z. Solvent-Induced Transformation of Single Crystals of a Spin-Crossover (SCO) Compound to Single Crystals with Two Distinct SCO Centers. *J. Am. Chem. Soc.* **2010**, *132*, 1558–1566. (d) Wei, R. J.; Li, B.; Tao, J.; Huang, R. B.; Zheng, L. S.; Zheng, Z. Making Spin-Crossover Crystals by Successive Polymorphic Transformations. *Inorg. Chem.* **2011**, *50*, 1170–1172. (e) Wei, R. J.; Tao, J.; Huang, R. B.; Zheng, L. S. Reversible and Irreversible Vapor-Induced Guest Molecule Exchange in Spin-Crossover Compounds. *Inorg. Chem.* **2011**, *50*, 8553–8564.
- (7) (a) Bréfuel, N.; Shova, S.; Lipkowski, J.; Tuchagues, J. P. Fe<sup>II</sup> Bistable Materials Based on Dissymmetrical Ligands: N<sub>4</sub> Schiff Bases Including 2-Pyridyl and 5-Methylimidazol-4-yl Rings Yield Various Fe<sup>II</sup> Spin-Crossover Phenomena around 300 K. *Chem. Mater.* **2006**, *18*, 5467–5479. (b) Bréfuel, N.; Shova, S.; Tuchagues, J. P. Fe<sup>II</sup> Bistable Materials with Dissymmetrical Ligands: Synthesis, Crystal Structure, Magnetic and Mössbauer Properties of Fe<sup>II</sup> Complexes Based on N<sub>4</sub> Schiff Bases Possessing 2-Pyridyl and 1-R-Imidazol-2-yl Rings. *Eur. J. Inorg. Chem.* **2007**, 4326–4334. (c) Bréfuel, N.; Vang, L.; Shova, S.; Dahan, F.; Costes, J. P.; Tuchagues, J. P. Fe<sup>II</sup> Spin Crossover Materials Based on Dissymmetrical N<sub>4</sub> Schiff Bases Including 2-Pyridyl and 2R-imidazol-4-yl Rings: Synthesis, Crystal Structure and Magnetic and Mössbauer Properties. *Polyhedron* **2007**, *26*, 1745–1757. (d) Hagiwara, H.; Okada, S. A Polymorphism-dependent T<sub>1/2</sub> Shift of 100 K in a Hysteretic Spin-Crossover Complex Related to Differences in Intermolecular Weak CH...X Hydrogen Bonds (X = S vs. S and N). *Chem. Commun.* **2016**, *52*, 815–818.
- (8) (a) Costa, J. S.; Lappalainen, K.; de Ruiter, G.; Quesada, M.; Tang, J. K.; Mutikainen, I.; Turpeinen, U.; Grunert, C. M.; Gütllich, P.; Lazar, H. Z.; Létard, J. F.; Gamez, P.; Reedijk, J. Remarkable Steric Effects and Influence of Monodentate Axial Ligands L on the Spin-Crossover Properties of trans-[Fe<sup>II</sup>(N<sub>4</sub> ligand)L] Complexes. *Inorg. Chem.* **2007**, *46*, 4079–4089. (b) Bonnet, S.; Siegler, M. A.; Costa, J. S.; Molnár, G.; Bousseksou, A.; Spek, A. L.; Gamez, P.; Reedijk, J. A Two-Step Spin Crossover Mononuclear Iron(II) Complex with a [HS–LS–LS] Intermediate Phase. *Chem. Commun.* **2008**, 5619–5621. (c) Castillo, Z. A.; Zheng, S.; Siegler, M. A.; Roubeau, O.; Bedoui, S.; Bonnet, S. Tuning the Transition Temperature and Cooperativity of bapbpy-Based Mononuclear Spin-Crossover Compounds: Interplay between Molecular and Crystal Engineering. *Chem. - Eur. J.* **2011**, *17*, 14826–14836. (d) Zheng, S.; Siegler, M. A.; Roubeau, O.; Bonnet, S. Influence of Selenocyanate Ligands on the Transition Temperature and Cooperativity of bapbpy-Based Fe(II) Spin-Crossover Compounds. *Inorg. Chem.* **2014**, *53*, 13162–13173.
- (9) (a) Lennartson, A.; Bond, A. D.; Piligkos, S.; McKenzie, C. J. Four-Site Cooperative Spin Crossover in a Mononuclear Fe<sup>II</sup> Complex. *Angew. Chem., Int. Ed.* **2012**, *51*, 11049–11052. (b) Arroyave, A.; Lennartson, A.; Dragulescu-Andrasi, A.; Pedersen, K. S.; Piligkos, S.; Stoian, S. A.; Greer, S. M.; Pak, C.; Hietsoi, O.; Phan, H.; Hill, S.; McKenzie, C. J.; Shatruck, M. Spin Crossover in Fe(II) Complexes with N<sub>4</sub>S<sub>2</sub> Coordination. *Inorg. Chem.* **2016**, *55*, 5904–5913.
- (10) Létard, J. F.; Asthana, S.; Shepherd, H. J.; Guionneau, P.; Goeta, A. E.; Suemura, N.; Ishikawa, R.; Kaizaki, S. Photomagnetism of a *syn-cis*-Dithiocyanato Iron(II) Complex with a Tetradentate N,N'-Bis(2-pyridylmethyl)1,2-ethanediamine Ligand. *Chem. - Eur. J.* **2012**, *18*, 5924–5934.
- (11) Zhou, J.; Zhu, B. W.; Luan, J.; Liu, Z.; Fang, J. K.; Bao, X.; Peng, G.; Tucek, J.; Bao, S. S.; Zheng, L. M. In Air a Spin Crossover Active Iron(II) Complex of Amine/NCBH<sub>3</sub><sup>-</sup> Ligands is Converted to a Low Spin Complex of Imine/CN<sup>-</sup> Ligands. *Dalton Trans.* **2015**, *44*, 20551–20561.
- (12) Luan, J.; Zhou, J.; Liu, Z.; Zhu, B. W.; Wang, H. S.; Bao, X.; Liu, W.; Tong, M. L.; Peng, G.; Peng, H.; Salmon, L.; Bousseksou, A. Polymorphism-Dependent Spin-Crossover: Hysteretic Two-Step Spin Transition with an Ordered [HS–HS–LS] Intermediate Phase. *Inorg. Chem.* **2015**, *54*, 5145–5147.
- (13) (a) Mohammed, R.; Chastanet, G.; Tuna, F.; Malkin, T. L.; Barrett, S. A.; Kilner, C. A.; Létard, J.-F.; Halcrow, M. A. Synthesis of 2,6-Di(pyrazol-1-yl)pyrazine Derivatives and the Spin-State Behavior of Their Iron(II) Complexes. *Eur. J. Inorg. Chem.* **2013**, 819–831. (b) Hogue, R. W.; Miller, R. G.; White, N. G.; Feltham, H. L. C.; Jameson, G. N. L.; Brooker, S. Hysteretic Spin Crossover in Iron(II) Complexes of a New Pyridine–Triazole–Pyrazine Ligand is Tuned by Choice of NCE co-Ligand. *Chem. Commun.* **2014**, *50*, 1435–1437.
- (14) Ali, K. A.; Elsayed, M. A.; Ragab, E. A. Catalyst Free Synthesis of Pyridine-2, 6-Bis (2-bromo-propane-1,3-dione) and Pyridine-2,6-

- bis(*N*-arylthiazoline-2-thiones). *Green Sustainable Chem.* **2015**, *5*, 39–45.
- (15) Sheldrick, G. M. A Short History of SHELX. *Acta Crystallogr., Sect. A: Found. Crystallogr.* **2008**, *64*, 112–122.
- (16) Dolomanov, O.; Bourhis, L. J.; Gildea, R. J.; Howard, J. A. K.; Puschmann, H. OLEX2: a Complete Structure Solution, Refinement and Analysis Program. *J. Appl. Crystallogr.* **2009**, *42*, 339–341.
- (17) (a) König, E.; Madeja, K.  $^5T_2-^1A_1$  Equilibriums in Some Iron(II)-Bis(1, 10-Phenanthroline) Complexes. *Inorg. Chem.* **1967**, *6*, 48–55. (b) Gobeze, W. A.; Milway, V. A.; Olguín, J.; Jameson, G. N. L.; Brooker, S. Nine Diiron(II) Complexes of Three Bis-tetradentate Pyrimidine Based Ligands with NCE (E = S, Se, BH<sub>3</sub>) Coligands. *Inorg. Chem.* **2012**, *51*, 9056–9065.
- (18) (a) Schneider, C. J.; Cashion, J. D.; Chilton, N. F.; Etrillard, C.; Fuentealba, M.; Howard, J. A. K.; Létard, J.-F.; Milsmann, C.; Moubaraki, B.; Sparkes, H. A.; Batten, S. R.; Murray, K. S. Spin Crossover in a 3,5-Bis(2-pyridyl)-1,2,4-triazolate-Bridged Dinuclear Iron(II) Complex  $[\{Fe(NCBH_3)(py)\}_2(\mu-L^1)]_2$  – Powder versus Single Crystal Study. *Eur. J. Inorg. Chem.* **2013**, *2013*, 850–864. (b) de Gaetano, Y.; Jeanneau, E.; Verat, A.; Yu; Rechinat, L.; Bousseksou, A.; Matouzenko, G. S. Ligand-Induced Distortions and Magneto-Structural Correlations in a Family of Dinuclear Spin Crossover Compounds with Bipyridyl-Like Bridging Ligands. *Eur. J. Inorg. Chem.* **2013**, 1015–1023. (c) Scott, H. S.; Ross, T. M.; Phonsri, W.; Moubaraki, B.; Chastanet, G.; Létard, J.-F.; Batten, S. R.; Murray, K. S. Discrete Fe<sup>II</sup> Spin-Crossover Complexes of 2,2'-Dipyridylamino-Substituted *s*-Triazine Ligands with Phenoxo, Cyanophenoxo and Dibenzylamino Functionalities. *Eur. J. Inorg. Chem.* **2015**, *2015*, 763–777. (d) Wu, X.-R.; Shi, H.-Y.; Wei, R.-J.; Li, J.; Zheng, L.-S.; Tao, J. Coligand and Solvent Effects on the Architectures and Spin-Crossover Properties of (4,4)-Connected Iron(II) Coordination Polymers. *Inorg. Chem.* **2015**, *54*, 3773–3780.
- (19) Klingele, J.; Kaase, D.; Klingele, M. H.; Lach, J. Synthesis and Mononuclear Complexes of the Bis-Bidentate Ligand 2,5-Di(2-Pyridyl)-1,3,4-Thiadiazole (dptd): Spin Crossover in  $[Fe^{II}(dptd)_2(NCSe)_2]$  and  $[Fe^{II}(dptd)_2(NCBH_3)_2] \cdot H_2O$ . *Dalton Trans.* **2012**, *41*, 1397–1406.
- (20) (a) Guionneau, P.; Marchivie, M.; Bravic, G.; Létard, J.-F.; Chasseau, D. Co(II) Molecular Complexes as a Reference for the Spin Crossover in Fe(II) Analogues. *J. Mater. Chem.* **2002**, *12*, 2546–2551. (b) Guionneau, P.; Marchivie, M.; Bravic, G.; Létard, J. F.; Chasseau, D. Structural Aspects of Spin Crossover. Example of the  $[Fe^{II}L_n(NCS)_2]$  Complexes. *Top. Curr. Chem.* **2004**, *234*, 97–128. (c) Marchivie, M.; Guionneau, P.; Létard, J.-F.; Chasseau, D. Photo-Induced Spin-Transition: The Role of the iron(II) Environment Distortion. *Acta Crystallogr., Sect. B: Struct. Sci.* **2005**, *61* (1), 25–28.
- (21) Phan, H. V.; Chakraborty, P.; Chen, M.; Calm, Y. M.; Kovnir, K.; Keniley, L. K., Jr.; Hoyt, J. M.; Knowles, E. S.; Besnard, C.; Meisel, M. W.; Hauser, A.; Achim, C.; Shatruk, M. Heteroleptic Fe<sup>II</sup> Complexes of 2,2'-Biimidazole and Its Alkylated Derivatives: Spin-Crossover and Photomagnetic Behavior. *Chem. - Eur. J.* **2012**, *18*, 15805–15815.
- (22) Sorai, M.; Seki, S. Phonon Coupled Cooperative Low-Spin  $^1A_1$  high-Spin  $^5T_2$  Transition in  $[Fe(phen)_2(NCS)_2]$  and  $[Fe(phen)_2(NCSe)_2]$  Crystals. *J. Phys. Chem. Solids* **1974**, *35* (4), 555–570.
- (23) Šalitraš, I.; Madhu, N. T.; Boča, R.; Pavlik, P.; Ruben, M. Room-Temperature Spin-Transition Iron Compounds. *Monatsh. Chem.* **2009**, *140*, 695–733.
- (24) Thompson, J. R.; Archer, R. J.; Hawes, C. S.; Ferguson, A.; Wattiaux, A.; Mathonière, C.; Clérac, R.; Kruger, P. E. Thermally and Photo-Induced Spin Crossover Behaviour in an Fe(II) Imidazolylamine Complex:  $[FeL_3](ClO_4)_2$ . *Dalton Trans.* **2012**, *41*, 12720–12725.